Suppression of carbon desorption from 4H-SiC by irradiating a remote nitrogen plasma at a low temperature

Masaharu Shimabayashi[1]*, Kazuaki Kurihara[2], and Koichi Sasaki[1]

[1] *Division of Quantum Science and Engineering, Hokkaido University, Sapporo 060-8628, Japan*
[2] *Toshiba Memory Corporation, Kapeldreef 75, 3001 Leuven Belgium*

We remotely irradiated a nitrogen plasma onto the carbon-side surface of 4H-SiC at a low temperature, and examined the effect of sample cooling on the characteristics of the nitride layer. An improved nitride layer, which had higher concentrations of carbon and silicon and a lower concentration of oxygen, was formed in the region at depths of more than 0.6-0.9 nm from the top surface. The depth of the fragile nitride layer in the top region, where no improved characteristics of the nitride layer were observed, became smaller with sample cooling. In addition, on the basis of the experimental results, we discussed the difference in the activation energy of the nitriding reaction of 4H-SiC supported by atomic nitrogen and molecular nitrogen in the metastable $A^3\Sigma_u^+$ state.

1. Introduction

The performance of Si-based power transistors has been reaching its theoretical limit in recent years.[1–4] For this reason, expectation is focused on SiC as a next-generation semiconductor, which has a high insulation voltage and robustness against high temperatures.[5–9] In addition, SiC-based metal-oxide-semiconductor field-effect transistors (MOSFETs) have potential advantages in terms of their low on-resistance and high switching speed.[10–16] However, the on-resistance of SiC-based MOSFETs under development is much higher than the theoretical expectation, which results in a large voltage drop, significant heat generation, and a low efficiency of electric power systems.

The high on-resistance of SiC-based MOSFETs is caused by the low mobility of carriers in the channel region under the gate insulation film. This low mobility is considered to be due to defects around the interface between the channel region and the gate insulation film.[17–23] Therefore, a method is required to passivate the surface of SiC before depositing the gate insulation film. A solution to this issue, which has been proposed on the basis of a first-principles calculation, is the nitriding of the SiC surface.[24] This patented proposed solution

*E-mail: shima@athena.qe.eng.hokudai.ac.jp

involves the formation of a monolayer of nitrogen atoms, which terminate surface dangling bonds, but a similar passivation function may be realized by a nitride layer of SiC with a limited thickness.

In a previous work, we examined the atomic concentrations of SiC surfaces remotely irradiated with nitrogen plasmas.[25] We observed the formation of a nitride layer with a thickness of 1-3 nm. In addition, the thickness of the nitride layer was greater when molecular nitrogen in the metastable $A^3\Sigma_u^+$ state was supplied from the plasma. However, the SiC surface remotely irradiated with nitrogen plasma had a lower weight density than virgin SiC. In particular, a decrease in the concentration of carbon was observed on the top surface of the sample. These experimental results suggest the removal of carbon from the SiC surface due to the desorption of volatile nitride molecules, such as C_2N_2, when the SiC surface is irradiated with reactive nitrogen species.

In this work, we controlled the temperature of SiC to be low during the irradiation of the remote nitrogen plasma. The aim of sample cooling was to prevent the desorption of volatile molecules. Since the vapor pressure of C_2N_2 is negligible at a temperature below -100 °C, it is expected that the desorption rate of volatile molecules is reduced by the low temperature. The idea of sample cooling was adopted successfully to reduce the etching rates of side walls in plasma-based dry etching.[26] This work shows that sample cooling also improves the characteristics of the surface passivated with plasmas.

2. Experimental procedure

The experimental apparatus is schematically shown in Fig. 1. The apparatus used in the present experiment was basically the same as that used in our previous work[25] except for the following two points. One was the use of p-BN as the discharge tube, instead of quartz in the previous work. The inner diameter of the p-BN tube was 8 mm, which was the same as that of the quartz tube. The other was the temperature of the sample, which is denoted by T_s in the following description. In this work, we installed a container that was filled with liquid nitrogen inside the chamber. The sample holder was connected to the container of liquid nitrogen using a copper ribbon. When nitrogen gas was not introduced into the chamber, the sample temperature decreased to $T_s \leq -150$ °C. The temperature increased when the gas was introduced and the plasma was produced. We controlled the sample temperature within specified ranges ($-63 \leq T_s \leq -58$ °C and $-145 \leq T_s \leq -117$ °C) by irradiating the plasma intermittently. The unit duration of the plasma irradiation was 5 min. We repeated the sample cooling and the plasma irradiation four times, and the total duration of the plasma irradiation

was 20 min in this experiment.

The other experimental apparatus and procedures were the same as those in our previous work.[25] A microwave power of 2.45 GHz was applied to a microwave resonator attached on the outside of the p-BN tube. The microwave power was 100 W. The distances (Z) between the microwave resonator and the sample were 7 and 12 cm. The chamber was evacuated using a turbomolecular pump to below 5×10^{-8} Torr before feeding nitrogen gas. Pure nitrogen gas was fed from the top of the p-BN tube at a flow rate of 288 ccm, and the nitrogen pressure in the chamber was adjusted to 0.5 Torr by reducing the pumping speed using a gate valve. A load lock chamber was attached to the side of the main chamber. A 4H-SiC sample with a size of 14×14 mm^2 was installed in the load lock chamber and was transferred to the sample holder in the main chamber. The sample was pretreated with 5% hydrogen fluoride solution for 10 min. We examined the nitriding characteristics of the carbon-side surface (C-face) of 4H-SiC.[27,28] The sample remotely irradiated with the nitrogen plasma was transferred back to the load lock chamber. The sample was kept in nitrogen atmosphere in the load lock chamber until it returned to room temperature. After that, the sample was exposed to the atmosphere and was transferred to analytical equipment. The analyses we used in this work were X-ray photoelectron spectroscopy (XPS) and high-resolution Rutherford backscattering (HRRBS).

3. Results

Figure 2 shows the depth profiles of atomic concentrations, which were obtained by HRRBS analyses, at the center of the C-face of SiC remotely irradiated with the nitrogen plasma. The distance Z was 12 cm. The temperatures of the sample were controlled at room temperature, between -63 and -58 °C, and between -145 and -117 °C [Figs. 2(a)-2(c), respectively]. The carbon concentration (100%) at the top surface is due to contamination. As shown in the figures, a nitride layer with a depth of $\sim$ 1.5 nm was formed on the sample surface. The depth profiles of the atomic concentrations shown in Fig. 3 were obtained when Z = 7 cm. The samples were controlled at the same temperatures as those in Fig. 2. As has been reported in our previous paper,[25] thicker nitride layers ($\sim$ 2.5 nm) were obtained by placing the microwave resonator closer to the sample. A high oxygen concentration and a low carbon concentration were observed at the top surface in both Figs. 2 and 3, which were the same results as those reported in the previous paper.

Figures 4 and 5 were obtained by averaging the atomic concentrations shown in Figs. 2 and 3 in the three depth regions from the top surface. The data at the top surface are excluded from the averaging procedure because of contamination. As shown in Fig. 4(a), when the

distance Z was 12 cm, the atomic concentrations in the depth region of $0.2 \leq d \leq 0.6$ nm were almost independent of the sample temperature. The concentration of carbon was extremely low, and the material in this depth region was similar to SiO_2. On the other hand, in the depth region of $0.6 \leq d \leq 1.0$ nm, we observed a decrease in the concentration of oxygen with the decrease in the sample temperature, as shown in Fig. 4(b), whereas the concentrations of carbon and silicon increased. The same trends were also observed in the depth region of $1.0 \leq d \leq 1.4$ nm, as shown in Fig. 4(c). The concentration of nitrogen was roughly independent of the sample temperature when $Z = 12$ cm. When the distance Z was 7 cm, the improvement in the atomic concentrations (namely, the decrease and the increase in the concentrations of oxygen and carbon, respectively) was also observed in the deep region of the sample, as shown in Fig. 5. No effect of sample cooling was observed in the depth region of $0.2 \leq d \leq 0.9$ nm [Fig. 5(a)]. The increase in carbon concentration was observed in the depth region of $0.9 \leq d \leq 1.6$ nm, but the oxygen concentration was constant in this region [Fig. 5(b)]. We observed the increase in carbon concentration and the decrease in oxygen concentration with the decrease in sample temperature in the depth region of $1.6 \leq d \leq 2.3$ nm, as shown in Fig. 5(c). It is noted here that the nitrogen concentration was decreased by sample cooling when the distance Z was 7 cm.

Figure 6 shows the XPS spectra of the N 1s peak, which were observed on the samples prepared at various temperatures. The spectra were obtained with Al Kα excitation and the take-off angle of the photoelectrons was 45^o. The distance Z was 12 cm. The spectra were deconvoluted by assuming two peaks corresponding to the N-Si and N-O_x bondings.[29] As shown in the figure, the N-Si bonding component became more dominant with the decrease in sample temperature. In addition, the width of the N-O_x peak decreased with the decrease in sample temperature. On the other hand, as shown in Fig. 7, the N-O_x bonding component became more dominant with the decrease in the temperature of the sample prepared at $Z = 7$ cm.

4. Discussion

The characteristics of the surface nitriding of SiC obtained by the present experiment were basically consistent with those reported in our previous paper.[25] We have reported that the sample is irradiated with atomic nitrogen when $Z = 12$ cm, whereas the mixture of atomic nitrogen and molecular nitrogen at the metastable $A^3\Sigma_u^+$ state irradiates the sample when $Z = 7$ cm.[30] On the other hand, the flux of N_2^+ was two orders of magnitude lower than those of atomic nitrogen and $N_2(A^3\Sigma_u^+)$ at both $Z = 12$ and 7 cm, indicating the negligible

contribution of N_2^+ to the nitriding of SiC. The deeper nitride layer synthesized at $Z = 7$ cm indicates that molecular nitrogen in the metastable $A^3\Sigma_u^+$ state has higher efficiency than atomic nitrogen for the surface nitriding of SiC, which is a major conclusion of the previous paper.

In this paper, we discuss the effect of the sample cooling on the nitriding characteristics of SiC. As can be seen from Figs. 4 and 5, the increases in carbon and silicon concentrations and the decrease in oxygen concentration with the decrease in sample temperature were observed in the middle region ($0.6 \leq d \leq 1.0$ nm when $Z = 12$ cm and $0.9 \leq d \leq 1.6$ nm when $Z = 7$ cm) and the bottom region ($1.0 \leq d \leq 1.4$ nm when $Z = 12$ cm and $1.6 \leq d \leq 2.3$ nm when $Z = 7$ cm) of the nitride layer. No such positive effects of sample cooling were observed in the top region ($0.2 \leq d \leq 0.6$ nm when $Z = 12$ cm and $0.2 \leq d \leq 0.9$ nm when $Z = 7$ cm). The positive effects were consistent with the XPS spectra shown in Fig. 6, which indicates the reduction of the N-O_x bonding component by sample cooling when $Z = 12$ cm. No reduction of the N-O_x bonding component was observed when $Z = 12$ cm, as shown in Fig. 7, but the discrepancy between the results of HRRBS (Fig. 5) and XPS is attributed to the fact that the improved nitride layer was buried in the deep region of the sample when $Z = 7$ cm. Since the escape lengths of photoelectrons produced by X-ray irradiation are 2.0 and 2.9 nm in SiC and SiO_2, respectively, the information obtained by XPS analysis mainly comes from the top region of the sample.

It is noted that the nitrogen concentration increases with the depth from the top surface in all the samples, as shown in Figs. 2 and 3. Since nitrogen atoms are transported from the plasma into the sample, it is speculated that the nitrogen concentration peak is located at the top surface during the irradiation of the plasma, and the depth profiles of the nitrogen concentration shown in Figs. 2 and 3 are formed when the samples are exposed to the atmosphere. Nitrogen atoms around the top surface are considered to be replaced by oxygen at the time of exposure to the atmosphere. That is, the experimental results suggest that the nitride layer formed in the top region is not robust enough to keep its chemical structure after its exposure to the atmosphere, even when it is synthesized at a low temperature (note that the sample temperature returns to room temperature when it is exposed to the atmosphere). On the basis of the aforementioned mechanism that determines the profile of the nitrogen concentration, the position of the nitrogen concentration peak represents the depth of the fragile nitride layer formed during plasma irradiation. It is understood by observing Figs. 2 and 3 carefully that the peak position of nitrogen concentration moves toward the top side by sample cooling, suggesting that the depth of the fragile nitride layer decreases. The increase in carbon con-

centration and the decrease in oxygen concentration are obtained in the region deeper than the nitrogen concentration peak, which may be caused by the suppression of the desorption of volatile reaction products such as C_2N_2 by the low temperature. In contrast to the peak position, the depth of the nitride layer is not affected with sample cooling, as shown in Figs. 2 and 3, suggesting that simple diffusion is not the dominant mechanism for the transport of nitrogen atoms in the sample.

It is interesting to note that the nitrogen concentration was not affected significantly by sample cooling when $Z = 12$ cm, as shown in Fig. 4, while the nitrogen concentration decreased with decreasing sample temperature when $Z = 7$ cm, as shown in Fig. 5. These contrasting experimental results give us a useful clue to the difference in the nitriding mechanisms of SiC by atomic nitrogen and molecular nitrogen in the metastable $A^3\Sigma_u^+$ state. According to these contrasting results, it can be concluded that molecular nitrogen in the metastable $A^3\Sigma_u^+$ state, which is supplied to the sample when $Z = 7$ cm, needs a higher thermal energy than atomic nitrogen to form the nitride layer on the SiC surface. That is, it is speculated that the activation energy of the nitriding reaction is higher for $N_2(A^3\Sigma_u^+)$ than for atomic nitrogen. This is reasonable since $N_2(A^3\Sigma_u^+)$ is only an electronic excited state and it returns to molecular nitrogen with no chemical reactivity after the decay of the excited energy on the sample surface. The activation energy of the nitriding reaction driven by atomic nitrogen is expected to be lower since atomic nitrogen is a radical species, resulting in the observation result that nitrogen concentration is not affected by sample temperature when $Z = 12$ cm.

5. Conclusions

In this work, we examined the effect of sample cooling on the nitriding characteristics of SiC using a remote nitrogen plasma. The experimental results indicate that an improved nitride layer, which had higher concentrations of carbon and silicon and a lower concentration of oxygen, was formed in a region with a distance of $d \geq 0.6$ nm ($Z = 12$ cm) and $d \geq 0.9$ nm ($Z = 7$ cm) from the top surface. Although the characteristics of the top region were not improved, the fragile nitride layer in the top region became thinner with sample cooling. In addition, the experimental results gave us a hint regarding in the differences in nitriding reactions supported by atomic nitrogen and molecular nitrogen in the metastable $A^3\Sigma_u^+$ state.

Acknowledgment

This work was supported by a Grant-in-Aid for JSPS Fellows (29001094).

References

1) B. J. Baliga, IEEE Electron Device Lett. **10**, 455 (1989).
2) F. Roccaforte, F. Giannazzo, F. Iucolano, J. Eriksson, M. H. Weng, and V. Raineri, Appl. Surf. Sci. **256**, 5727 (2010).
3) D. Han, J. Noppakunkajorn, and B. Sarlioglu, IEEE Trans. Veh. Technol. **63**, 3001 (2014).
4) T. J. Flack, B. N. Pushpakaran, and S. B. Bayne, J. Electron. Mater. **45**, 2673 (2016).
5) S. K. Powell, N. Goldsman, J. M. McGarrity, J. Bernstein, C. J. Scozzie, and A. Lelis, J. Appl. Phys. **92**, 4053 (2002).
6) L. C. Yu, G. T. Dunne, K. S. Matocha, K. P. Cheung, J. S. Suehle, and K. Sheng, IEEE Trans. Device Mater. Reliab. **10**, 418 (2010).
7) Y. K. Sharma, A. C. Ahyi, T. Issacs-Smith, X. Shen, and S. T. Pantelides, Solid State Electron. **68**, 103 (2012).
8) M. Alexandru, V. Banu, X. Jorda, J. Montserrat, M. Vellvehi, D. Tournier, J. Millan, and P. Godignon, IEEE Trans. Ind. Electron. **62**, 3182 (2015).
9) D. P. Sadik, G. Tolstoy, and J. Rabkowski, IEEE Trans. Ind. Electron. **63**, 1995 (2016).
10) J. Millan, P. Godignon, X. Perpina, A. Perez-Tomas, and J.Rebollo, IEEE Trans. Power Electron. **29**, 2155 (2014).
11) J. Fabre, P. Ladoux, and M. Piton, IEEE Trans. Power Electron. **30**, 4079 (2015).
12) B. Cougo, H. Schneider, and T. Meynard, IEEE Trans. Power Electron. **30**, 4489 (2015).
13) S. Dimitrijev, J. Han, H. A. Moghadam, and A. Aminbeidokhti, MRS Bull. **40**, 399 (2015).
14) K. Fukuda, D. Okamoto, M. Okamoto, T. Deguchi, T. Mizushima, K. Takenaka, H. Fujisawa, S. Harada, Y. Tanaka, Y. Yonezawa, T. Kato, S. Katakami, M. Arai, M. Takei, S. Matsunaga, K. Takao, T. Shinohe, T. Izumi, T. Hayashi, S. Ogata, K. Asano, H. Okumura, and T. Kimoto, IEEE Trans. Electron Devices **62**, 396 (2015).
15) S. Ryu, C. Capell, E. Van Brunt, C. Jonas, M. O ' Loughlin, J. Clayton, K. Lam, V. Pala, B. Hull, Y. Lemma, D. Lichtenwalner, Q. J. Zhang, J. Richmond, P. Butler, D. Grider, J. Casady, S. Allen, J. Palmour, M. Hinojosa, C. W. Tipton, and C. Scozzie, Semicond. Sci. Technol. **30**, 084001 (2015).
16) E. Gurpinar and A. Castellazzi, IEEE Trans. Power Electron. **31**, 7184 (2016).
17) G. Y. Chung, C. C. Tin, J. R. Williams, K. McDonald, M. Di Ventra, S. T. Pantelides, L.

C. Feldman, and R. A. Weller, Appl. Phys. Lett. **76**, 1713 (2000).

18) S. Wang, M. Di Ventra, S. G. Kim, and S. T. Pantelides, Phys. Rev. Lett. **86**, 5946 (2001).

19) J. L. Cantin, H. J. von Bardeleben, Y. Shishkin, Y. Ke, R. P. Devaty, and W. J. Choyke, Phys. Rev. Lett. **92**, 015502 (2004).

20) J. M. Knaup, P. Deak, T. Frauenheim, A. Gali, Z. Hajnal, and W. J. Choyke, Phys. Rev. B **71**, 235321 (2005).

21) P. Deak, J. M. Knaup, T. Hornos, C. Thill, A. Gali, and T. Frauenheim, J. Phys. D **40** 6242 (2007).

22) X. Shen and S. T. Pantelide, Appl. Phys. Lett. **98**, 053507 (2011).

23) C. J. Cochrane, P. M. Lenahan, and A. J. Lelis, J. Appl. Phys. **109**, 014506 (2011).

24) T. Shimizu and T. Shinohe, U.S. Patent 0,199,846A1 (2012).

25) M. Shimabayashi, K. Kurihara, and K. Sasaki, Jpn. J. Appl. Phys. **55**, 036503 (2016).

26) S. Tachi, K. Tsujimoto, and S. Okudaira, Appl. Phys. Lett. **52**, 616 (1988).

27) K. Fukuda, M. Kato, K. Kojima, and J. Senzaki, Appl. Phys. Lett. **84**, 2088 (2004).

28) T. Kimoto, Y. Kanzaki, M. Noborio, H. Kawano, and H. Matsunami, Jpn. J. Appl. Phys. **44**, 1213 (2005).

29) J. P. Chang, M. L. Green, V. M. Donnelly, R. L. Opila, J. Eng, Jr., J. Sapjeta, P. J. Silverman, B. Weir, H. C. Lu, T. Gustafsson, and E. Garfunkel, J. Appl. Phys. **87**, 4449 (2000).

30) Y. Horikawa, K. Kurihara, and K. Sasaki, Appl. Phys. Express **4**, 086201 (2011).

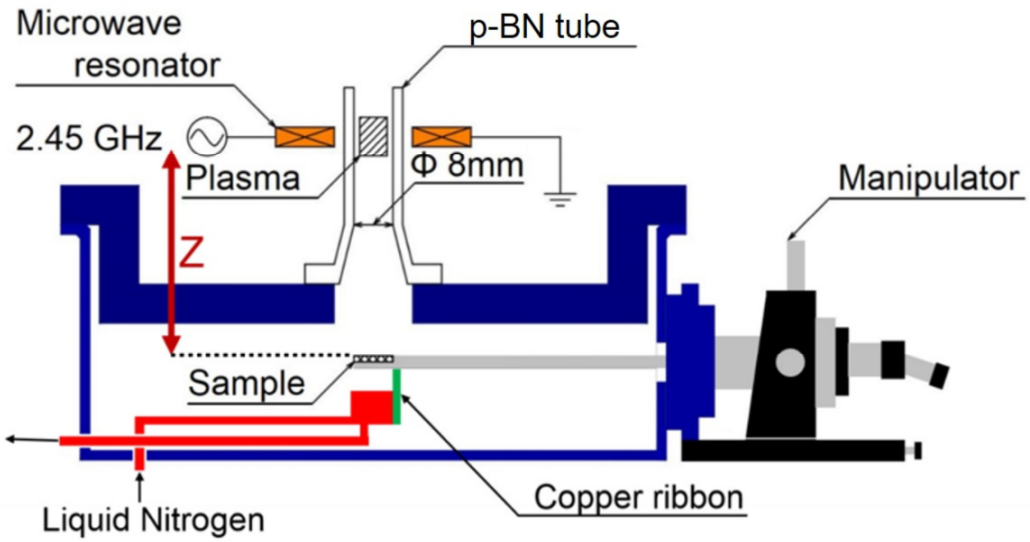

Fig. 1. Schematic diagram of the experimental apparatus.

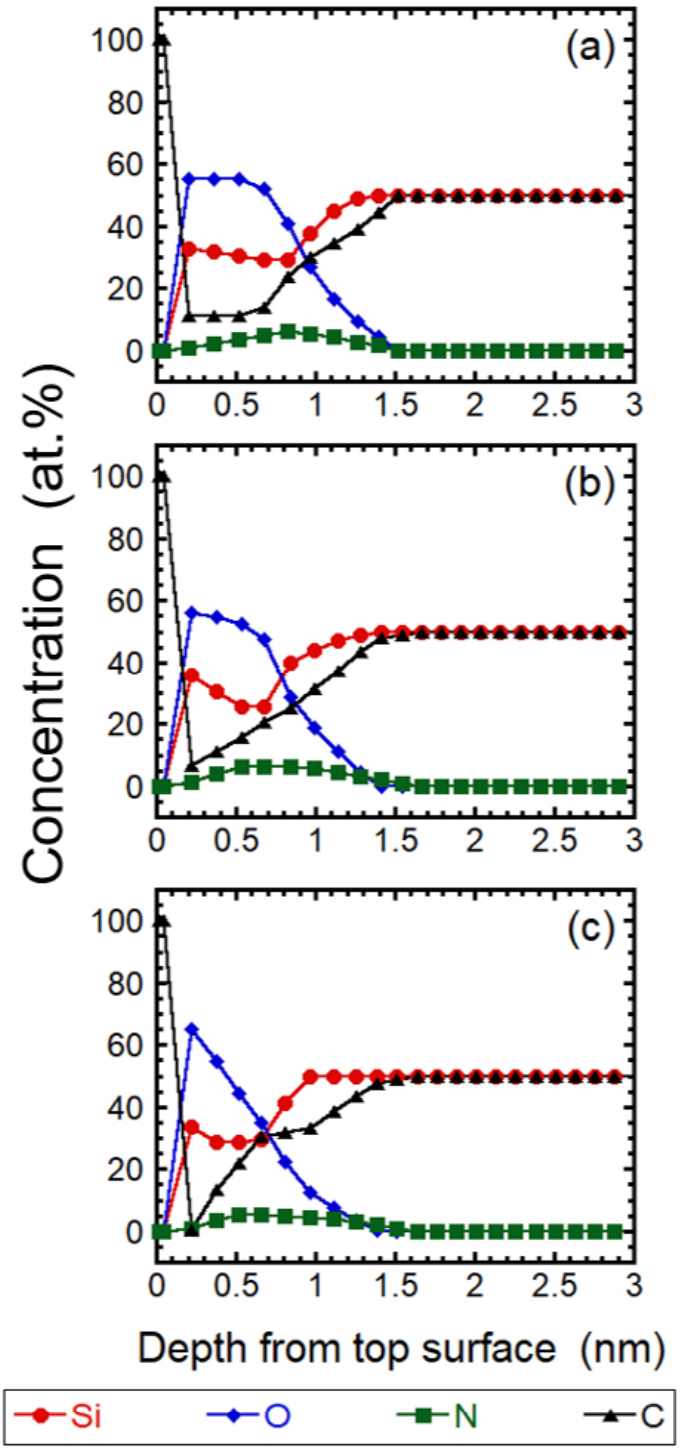

Fig. 2. Depth profiles of the atomic concentrations on the carbon-side surfaces of SiC remotely irradiated with the nitrogen plasma at (a) room temperature, (b) $-63 \leq T_s \leq -58$ °C, and (c) $-145 \leq T_s \leq -117$ °C. The distance Z was 12 cm.

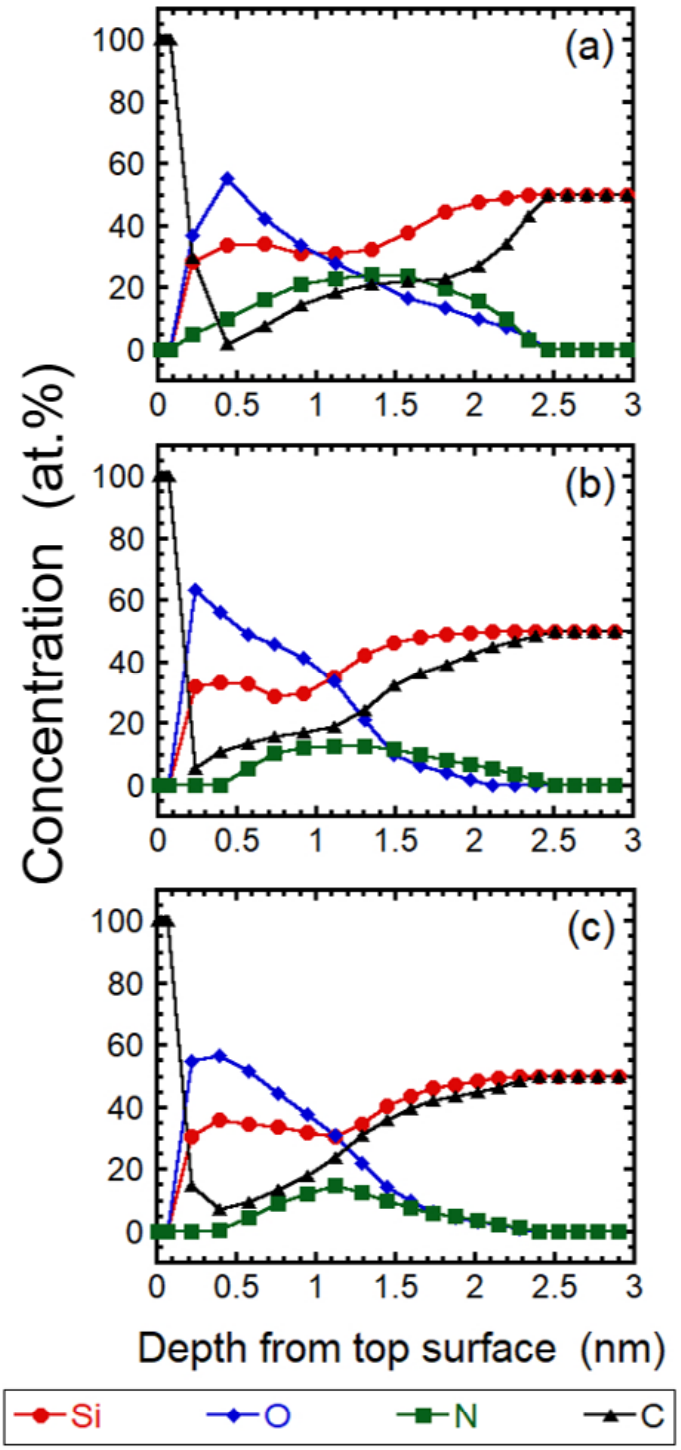

Fig. 3. Depth profiles of the atomic concentrations on the carbon-side surfaces of SiC remotely irradiated with the nitrogen plasma at (a) room temperature, (b) $-63 \leq T_s \leq -58$ °C, and (c) $-145 \leq T_s \leq -117$ °C. The distance Z was 7 cm.

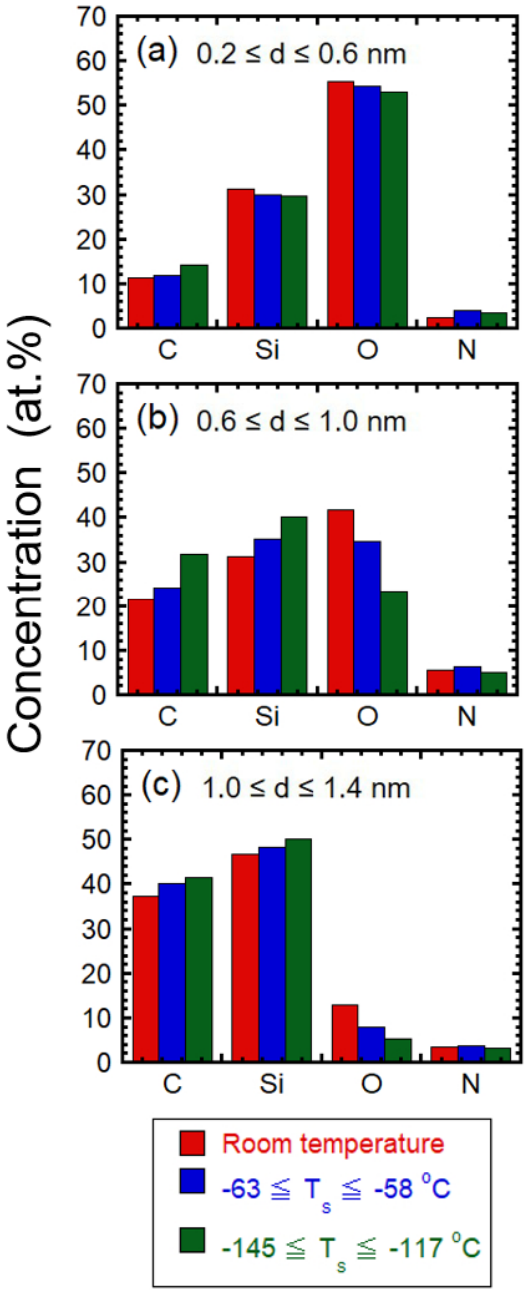

Fig. 4. Average concentrations of C, Si, O, and N in depth regions of (a) $0.2 \leq d \leq 0.6$ nm, (b) $0.6 \leq d \leq 1.0$ nm, and (c) $1.0 \leq d \leq 1.4$ nm as a function of sample temperature. The distance Z was 12 cm.

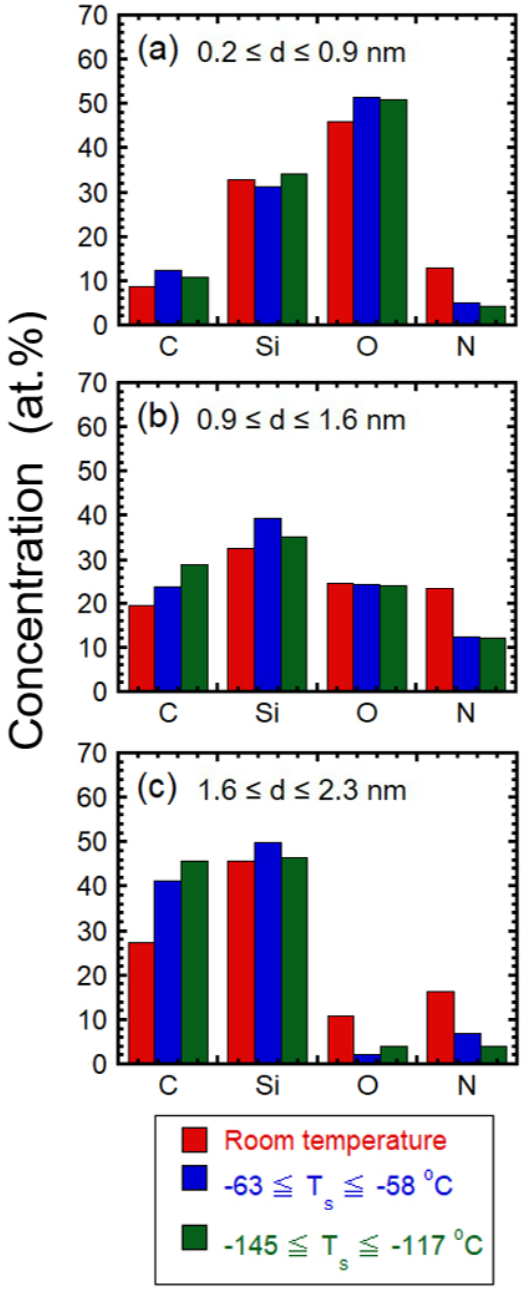

Fig. 5. Average concentrations of C, Si, O, and N in depth regions of (a) $0.2 \leq d \leq 0.9$ nm, (b) $0.9 \leq d \leq 1.6$ nm, and (c) $1.6 \leq d \leq 2.3$ nm as a function of sample temperature. The distance Z was 7 cm.

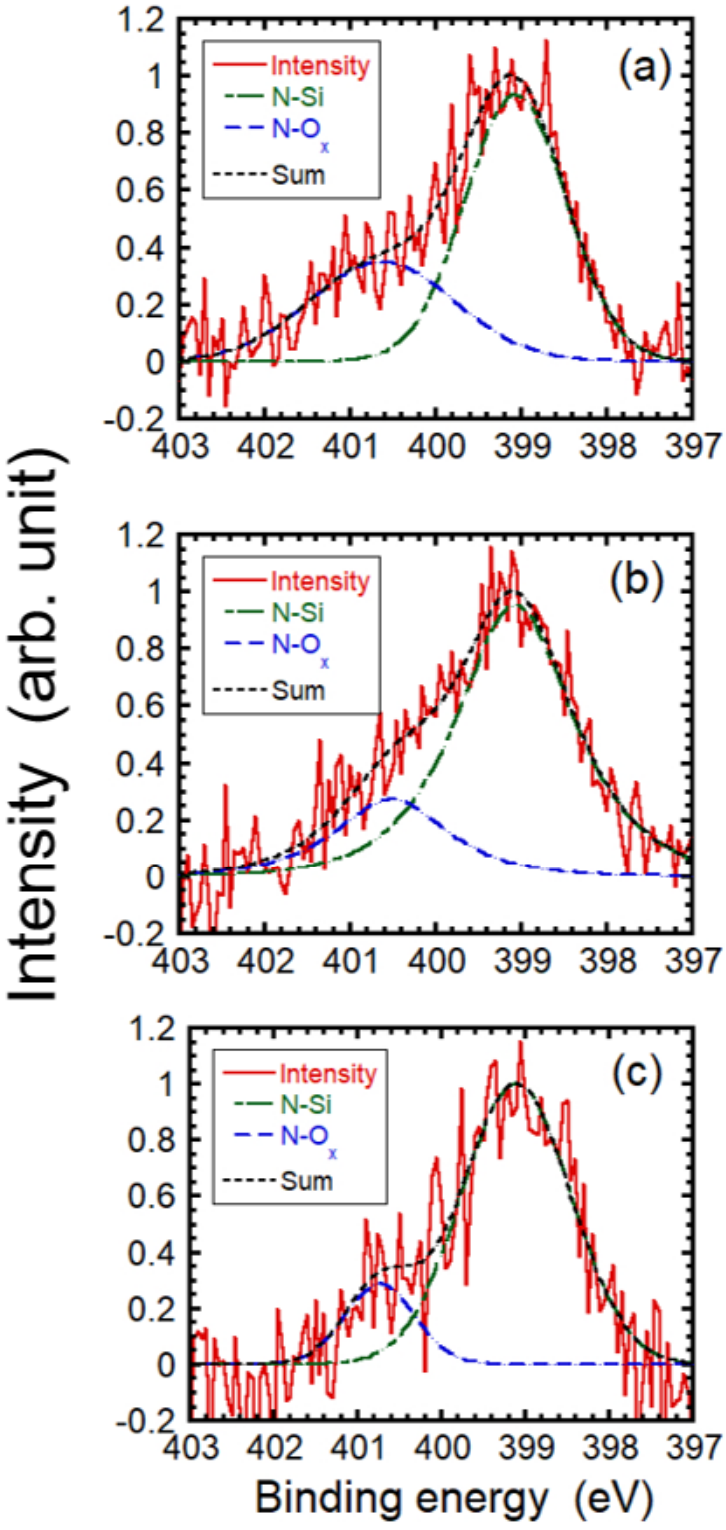

Fig. 6. XPS spectra of the N 1s peak observed on the sample surface prepared at (a) room temperature, (b) $-63 \leq T_s \leq -58$ °C, and (c) $-145 \leq T_s \leq -117$ °C. The distance Z was 12 cm.

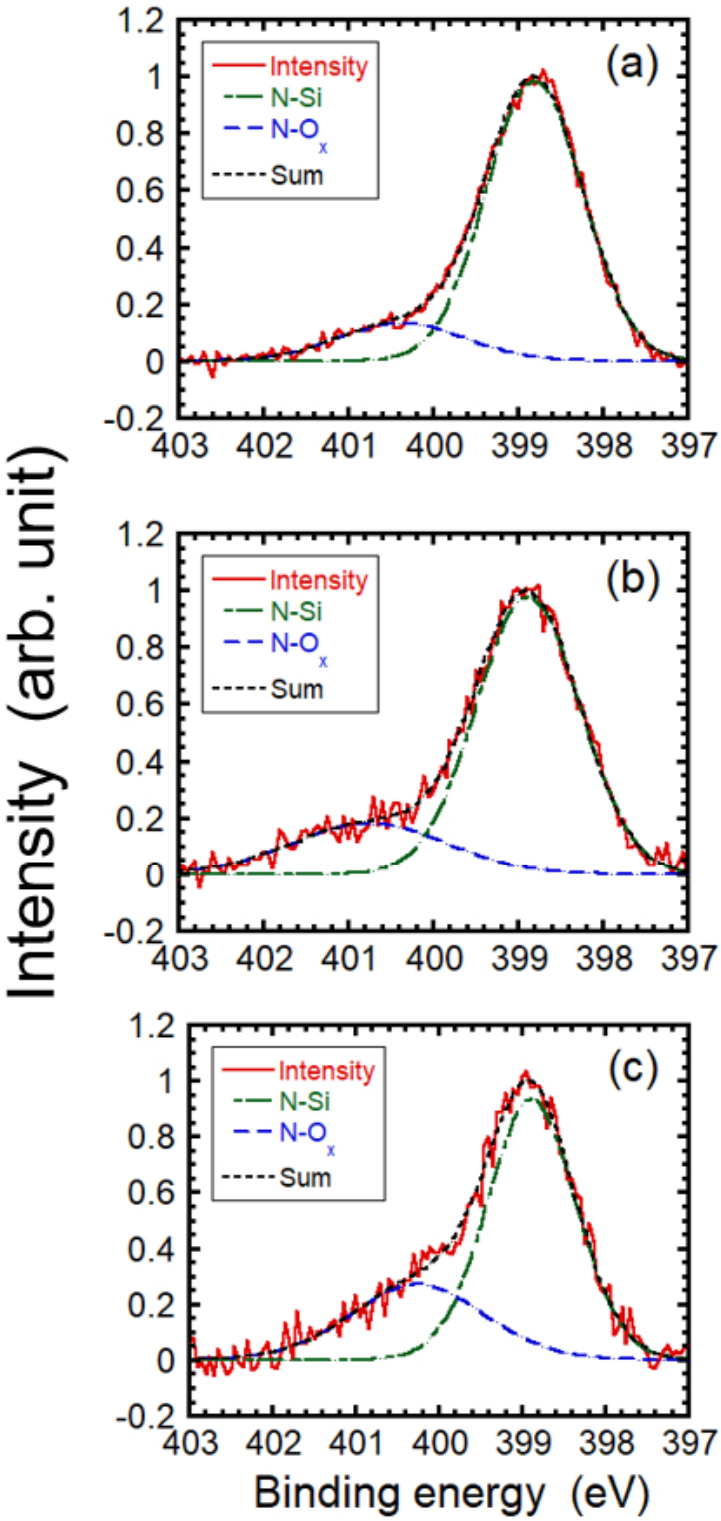

Fig. 7. XPS spectra of the N 1s peak observed on the sample surface prepared at (a) room temperature, (b) $-63 \leq T_s \leq -58$ °C, and (c) $-145 \leq T_s \leq -117$ °C. The distance Z was 7 cm.